Received 17 August 2023, accepted 11 September 2023, date of publication 20 September 2023,
date of current version 27 September 2023.

*Digital Object Identifier 10.1109/ACCESS.2023.3317431*

RESEARCH ARTICLE

# Advancing Multiband OFDM Channel Sounding: An Iterative Time Domain Estimation for Spectrally Constrained Systems

**ASIF IQBAL[1], MICHEAL DRIEBERG[1], (Member, IEEE), VARUN JEOTI[2], (Senior Member, IEEE), AZRINA ABD AZIZ[1], (Senior Member, IEEE), GORAN M. STOJANOVIĆ[2], (Member, IEEE), MITAR SIMIĆ[2], (Member, IEEE), AND NAZABAT HUSSAIN[3]**

[1]Department of Electrical and Electronic Engineering, Universiti Teknologi PETRONAS, Seri Iskandar 32610, Malaysia
[2]Faculty of Technical Sciences, University of Novi Sad, 21000 Novi Sad, Serbia
[3]GE Vingmed Ultrasound AS, 3183 Horten, Norway

Corresponding author: Asif Iqbal (asif.iqbal@msn.com)

This work was supported by the European Union's Horizon 2020 Research and Innovation Program under Grant 854194.

**ABSTRACT** The emerging wireless applications are facing new challenges in combating frequency congestion. As a result, the opportunistic utilization of available frequency spectrum and channel bonding is becoming increasingly common in new wireless standards. In these systems, the transmit waveforms are required to have nulls in specific frequency bands to avoid interference with primary users. However, these nulls can significantly affect the performance of channel estimation algorithms. Therefore, this work proposes a novel Iterative Multiband (MB) Spectrally Constrained Time-Domain (SCTD) technique to reduce the residual error of correlation due to spectrally constrained waveforms. The performance of the newly developed technique is evaluated through extensive numerical experiments, where the Mean Squared Error (MSE) and Bit Error Rate (BER) are computed for various scenarios. The accuracy of the proposed technique is compared with known channel state information and with conventional techniques. The simulation results show that the proposed Time-Domain Iterative Method, SCTD, performed better than conventional techniques for various Rayleigh channel conditions with Additive White Gaussian Noise (AWGN). It was found that after ten iterations, the proposed technique outperforms the conventional technique for both stationary and mobile frequency-selective channels. Furthermore, it was observed that the proposed SCTD technique requires fewer pilot signals to achieve a similar performance. The results show that the proposed SCTD method supersedes the conventional techniques for stationary and mobile frequency selective channel scenarios within ten iterations. Subsequently, it is observed that the proposed SCTD method requires 50% fewer pilots to provide similar performance compared to conventional methods. It is also observed that the proposed SCTD method provides an average of 6 dB mean squared error (MSE) advantage for low signal-to-noise ratio per bit ($E_b/N_0$) regime cases. It can be concluded that the proposed technique is highly suitable, particularly for low $E_b/N_0$ regimes and can be used for various communication systems.

**INDEX TERMS** Channel sounder, PAPR, channel impulse response, channel characteristics, 5G/6G, OFDM, MB-OFDM, spectrally constrained.

## I. INTRODUCTION

Over the past few years, channel sounding techniques have transitioned from being mere academic pursuits to vital tools in modern communication networks [1]. Channel sounding methods are pivotal in evaluating and understanding the wireless channel environment [2]. Whether it's for next-generation cellular systems or understanding the intricacies of complex environments, such as the 60-GHz range [3], these techniques play an essential role. At its core, channel

The associate editor coordinating the review of this manuscript and approving it for publication was Parul Garg.

sounding aims to obtain the channel impulse response (CIR) using specially designed probing signals to illuminate and characterize the channel. The transmitted waveforms interact with the scattering objects and create multiple time-delayed and phase variant copies. These distorted signals are then measured at the receiver to estimate the environmental conditions. These measurements are used to develop channel models, which help in designing robust modulation schemes for reliable communication systems.

Lately, the adaptive utilization of available frequency spectrum and channel bonding has become very common in new wireless standards [4]. Since the channel sounders require a large system bandwidth for better resolution, the opportunistic utilization of available frequency bands will be a new direction in ultrawideband (UWB) channel sounding. Among the most popular sounding methods, direct radio frequency (RF) pulse, sliding correlator, frequency swept, and orthogonal frequency-division multiplexing (OFDM) based systems [5], [6], [7] are a few of the most used techniques. OFDM offers various advantages, which include the flexibility of signal design and highly efficient digital signal processing. Recently, MB sounding schemes have been proposed for UWB channel sounding [8], [9], [10], [11]. MB-OFDM has proven to be a most attractive solution due to its design flexibility [11]. In MB systems, the total frequency band is divided into various sub-bands, and then information is processed in a smaller group, which significantly reduces the system cost complexity and provides spectral flexibility for international regulatory compliance. However, since the transmit waveforms must follow governance and standards, these nulls' shape, depth, and width have to meet the spectral criteria [12]. These nulls also result in significant performance degradation of channel estimation algorithms [13]. Thus, providing a low complexity channel estimation for spectrally constrained (SC) MB waveform is the focus of this work.

Conventionally, the channel estimation is performed either using preambles or with the assistance of pilots. Preamble-based channel estimation is more useful when the propagation channel is stationary. However, pilots-based techniques provide better performance in the dynamic channel [14], [15], [16], [17], [18], [19]. Pilot-assisted channel estimation techniques are usually characterized as time-domain (TD) or frequency-domain (FD) based on their primary domain of computation. In FD techniques, the most common methods are the least square (LS) and minimum mean square error (MMSE). LS technique is computationally efficient. However, it suffers from poor accuracy. On the other hand, the MMSE method minimizes the error of LS estimation. However, MMSE requires higher computation [20], [21]. Compared to FD methods, time-domain methods have received less attention. However, the low computation complexity design of TD makes them a strong candidate for the channel estimation [22]. In addition, TD estimation gives a robust performance in inter-carrier interference (ICI) scenarios. The TD channel estimation methods can generally be categorized into two types. Those employ discrete Fourier transform (DFT) processing to compute CIR from LS estimates [23], [24], [25], [26], [27], [28], and those utilize TD correlation between the received signal and known signal to estimate the CIR [13], [29], [30], [31], [32], [33].

Another time-domain method that is widely adopted is the Time domain synchronous OFDM (TDS-OFDM), which enhances spectral and energy efficiency. This improvement is achieved by replacing the traditional cyclic prefix or guard interval, used in conventional OFDM, with a known pseudo-random noise (PN) sequence. TDS-OFDM is renowned for its rapid synchronization and spectral efficiency. However, it faces challenges, notably inter-block interference in multipath channels. One study introduces a compressive sensing theory algorithm tailored for underwater channels, enhancing performance metrics such as bit error rate and energy efficiency [34]. Another approach replaces traditional methods in TDS-OFDM with a pseudorandom noise sequence, suggesting a novel training sequence for underwater channels [35]. This results in significant improvements in spectral and energy utilization. While TDS-OFDM showcases remarkable efficiencies, it struggles with high-order modulation in specific channel conditions. To address this, subsequent research proposes structured compressive sensing for multi-channel reconstruction [36]. Additionally, another study leverages compressive sensing theory to introduce a groundbreaking channel estimation method [37]. Collectively, these advancements support higher modulations and deliver superior performance across varied channel conditions. TDS-OFDM, while efficient for data transmission, is unsuitable for channel sounding due to its potential for pseudorandom noise interference, limited resolution in capturing dense multipath components, challenges in depicting fast-varying channels, risk of misinterpreting its unique features as channel characteristics, and the presence of inter-block interference.

TD correlation methods mostly utilize frequency-domain (FD) pilots for channel estimation One such technique is the frequency-domain pilot time-domain correlation (FPTC) method, which uses the correlation between known pilots and embedded pilots in the received signal to estimate the channel impulse response (CIR). FPTC has advantages such as a large dynamic range, simple implementation, and robustness against synchronization errors, but requires deconvolution, which is computationally intensive [38]. Other variations of the FPTC method include the frequency-domain pilots and time-domain processing (FPTP) method, which uses cyclic correlation and transform domain cyclic correlation to improve performance [39]. Some approaches, such as those proposed by Liu et al. [40] and Lin et al. [41], use superimposed pilot signals and windowing to improve performance, respectively. In a series of articles [13], [32], [42], Khan et al. proposed improved FPTC methods for single-carrier (SC) channels, such as the no guard band and virtual sub-carrier pilot signals method. A similar method, time-domain pilot-based channel estimation (TDPCE), uses adaptive algorithms and Kalman filtering to track time-varying multipath Rayleigh channels [43]. FPTC methods offer better performance, dynamic range, and computational complexity compared to DFT-based methods, but may not perform well in spectrally constrained scenarios.

Usually, both FD and TD estimation techniques provide an optimum performance when the pilots are uniformly distributed. However, for SC waveforms, various methods are proposed to improve channel estimation performance. Broadly, they can be categorized as optimal sequence design, pilot location, power optimization, virtual carriers insertion, and iterative schemes. In the optimal sequence design, efforts are made to develop a new SC sequence for desirable correlation properties [44], [45]. Pilot optimization techniques solve the problem by finding the optimal pilot location and power to meet the low peak-to-average power ratio (PAPR) and mean squared error (MSE) requirements [46], [47], [48], [49]. Another approach assumes virtual carriers and reduces the MSE within an acceptable range [50], [51], [52]. Lately, iterative methods have been introduced to minimize MSE. Iterative schemes proved to be less complicated and provide acceptable performance [13], [32], [53], [54].

Addressing the limitations of previous techniques, a new low complexity time-domain correlation-based iterative technique is proposed to reduce the residual error caused by the SC waveforms. It utilizes a constant amplitude zero autocorrelation waveform (CASAZ) family sequence that can provide a low PAPR MB-OFDM SC waveform [55].

The significant scientific contribution of this research work is the design of MB-OFDM channel estimation for SC channels. A new spectrally constrained CAZAC sequence-based phasing pilot sequence is utilized to provide low PAPR. A flexible architecture is adapted for the sounding system using MB-OFDM, while maintaining all the valuable properties of OFDM [55]. A novel iterative time-domain channel estimation, SCTD, is developed to reduce the residual correlation error due to SC waveforms. The performance of the proposed techniques is validated with extensive numerical experiments.

The remainder of this paper is organized as follows: Section II presents the overall methodology and signal design. Section III provides the formulation of the problem. Section IV explains the proposed spectrally constrained time-domain (SCTD) channel estimation, and Section V discusses MB CIR computation. Results and analysis are discussed in Section VI. Lastly, the conclusion of the work is presented.

## II. MULTIBAND OFDM PROBING SIGNAL

Consider a UWB system built by concatenating $S$ multiband, as shown in Figure 1. Each subband occupies a baseband signal bandwidth (BW), where software defined radio (SDR) hardware specifications define the signal BW. Each subband is further divided into $N$ orthogonal subcarriers.

An OFDM symbol, $x[n]$, is constructed from constellations at the frequency bins to a time-domain complex

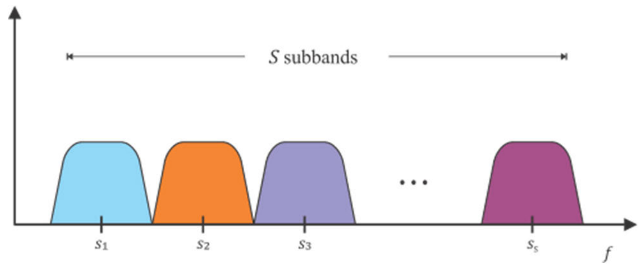


**FIGURE 1. UWB multiband OFDM spectrum.**

waveform using Inverse Fast Fourier Transform (IFFT). The resulting time-domain samples of OFDM symbol, $x_m[n]$, for $m^{\text{th}}$ period can be written as [56],

$$x_m[n] = \sum_{k=0}^{N-1} s_m[k] \, e^{j2\pi nk/N}, \tag{1}$$

where $s_m[k]$ represents a complex modulated symbol to be transmitted in subcarrier $k$. The frequency spacing between adjacent subcarriers is $\Delta f = BW/N$. Let $s_m[k] = c_m[k] + q_m[k]$, where $c_m[k]$ and $q_m[k]$ are complex-valued data and pilots tones transmitted in the $k^{\text{th}}$ subcarriers, respectively. Using (1), the time-domain samples of $m^{\text{th}}$ OFDM Symbol can be rewritten as,

$$x_m[n] = \sum_{k=0}^{N-1} (c_m[k] + q_m[k]) \, e^{j2\pi nk/N}. \tag{2}$$

Next, the time-domain complex baseband signal $x_m[n]$ is upconverted to a carrier frequency, $f_m$. The transmitted RF signal can be written as [56],

$$y(t) = \sum_{m} \mathrm{Re}\left[x_m\left(n - mT_{sym}\right) e^{j2\pi f_m t}\right], \tag{3}$$

where $f_m$ is the center frequency of subband for $m^{\text{th}}$ OFDM symbol duration. The carrier frequencies are selected based on pre-defined time-frequency codes.

The data tones, $c_m[k]$, are assigned from the QPSK or QAM constellations. Whereas, pilot tones, $q_m[k]$, are unity-gain phase-modulated tones that take values from sequences $p_m[u]$ as described below,

$$p_m[u] = a_m[u] \, e^{j\theta_m[u]} \tag{4}$$

where, $a_m[u]$ and $\theta_m[u]$ are amplitude and phase associated with $u^{\text{th}}$ element of sequence for $m$th symbol, and $j = \sqrt{-1}$ is an imaginary number.

In [55], the authors proposed a new low PAPR phasing scheme based on the Zadoff–Chu (ZC) sequence. In the proposed method, symbols are synthesized in the frequency domain, and phase randomization of pilot tones is performed using the phases from the ZC sequence. A ZC sequence is given by,

$$p_m^{Chu}[u] = a_m^{Chu}[u] \, e^{j\theta_m^{Chu}[u]} \tag{5}$$

In (5), $a_m^{Chu}$ is the amplitude and $\theta_m^{Chu}$ is the phase of the sequence, described as,

$$\theta_m^{Chu}[u] = -j\frac{\pi\gamma u(u+c_f+2\kappa)}{N_p} \tag{6}$$

where,
$0 \leq u < N_p$,
$0 < u < N_p$ and $\gcd(N_p, \gamma) = 1$,
$c_f = N_p \bmod 2$,
$\kappa \in \mathbb{Z}$, and
$N_p$ = length of the sequence.

### A. DERIVATION OF SPECTRALLY CONSTRAINED PILOT SEQUENCE

In the previous section, a perfect periodic ZC sequence is presented for pilot tones. However, in the practical implementation, the spectrum has data subcarriers to carry the data, guard subcarriers to avoid the spectrum leakages, and also a null DC subcarrier to avoid the impairments caused by the receiver imperfections. Similarly, in cognitive systems, the spectrum shaping is very dynamic to avoid interference between existing users. In these scenarios, the periodicity of the pilot tones cannot be maintained. In the proposed work, an aperiodic pilot tones phasing sequence can be derived from the periodic phasing sequence as follows:

Let $\boldsymbol{A}_{sub} = \{1, 2, 3, \ldots, N\}$ be a set of available frequency bin indices, and $N$ is FFT size. In an ideal case, if all subcarriers are available for pilot tones, the length of the sequence, $N_p$, will be equal to $N$ and the pilot tones, $\boldsymbol{q}_{k_p}$, for $m^{\text{th}}$ symbol are assigned from a perfect periodic complex-valued $\boldsymbol{p}_u$ sequence using (5) as,

$$\boldsymbol{q}_{m,k_p}^{per} = \boldsymbol{p}_{m,u_p^{per}}, \tag{7}$$

where $\boldsymbol{k}_p = \boldsymbol{A}_{sub}$, $\boldsymbol{u}_p^{per} = \{0, 1, 2, \ldots, N_p - 1\}$ and $\boldsymbol{m} = 0, 1, 2, \ldots, M_{sym} - 1$.

In the presence of guard, DC and data subcarriers, let, $\boldsymbol{B}_g$ be set the guard subcarriers indices where $\boldsymbol{B}_g \subset \boldsymbol{A}_{sub}$, and the DC subcarrier $\boldsymbol{B}_{dc} \in \boldsymbol{A}_{sub}$. The useable subcarrier subset can be written as,

$$\boldsymbol{A}_u = \boldsymbol{A}_{sub} \backslash \left(\boldsymbol{B}_g \cup \boldsymbol{B}_{dc}\right). \tag{8}$$

If the OFDM symbol contains no pilot tones, then the data carrier indices subset $\boldsymbol{k}_d \subseteq \boldsymbol{A}_u$, otherwise $\boldsymbol{k}_d \subset \boldsymbol{A}_u$ and the number of elements of $\boldsymbol{k}_d$ is equal to $N_d$. The indices subset of pilot tones is $\boldsymbol{k}_p = \boldsymbol{A}_u \backslash \boldsymbol{k}_d$. An aperiodic sequence $\boldsymbol{p}_{m,u_p^{aper}}$ is a subset of $\boldsymbol{p}_{m,u_p^{per}}$, with indices $\boldsymbol{u}_p^{aper} = \boldsymbol{k}_p - 1$. The length of the aperiodic sequence will be equal to $N_p$. Another aperiodic sequence named 'residual sequence', $\boldsymbol{p}_{m,u_p^{res}}$, is also derived from $\boldsymbol{p}_{m,u_p^{aper}}$, with indices $\boldsymbol{u}_p^{res} = \boldsymbol{k}_p \backslash \boldsymbol{u}_p^{aper}$. Hence, the periodic sequence, $\boldsymbol{p}_{m,u_p^{per}}$, can be written as,

$$\boldsymbol{p}_{m,u_p^{per}} = \boldsymbol{p}_{m,u_p^{aper}} + \boldsymbol{p}_{m,u_p^{res}}, \quad \text{where,} \\ \boldsymbol{u}_p^{aper} \neq \boldsymbol{u}_p^{res}. \tag{9}$$

For spectrally constrained cases, the pilot tones $\boldsymbol{q}_{k_p}$ for $m^{\text{th}}$ symbol are assigned from complex-valued aperiodic sequences, $\boldsymbol{p}_{u_p^{aper}}$ and $\boldsymbol{p}_{u_p^{res}}$ as,

$$\begin{aligned} \boldsymbol{q}_{m,k_p}^{aper} &= \boldsymbol{p}_{m,u_p^{aper}}, \\ \boldsymbol{q}_{m,k_p}^{res} &= \boldsymbol{p}_{m,u_p^{res}}. \end{aligned} \tag{10}$$

In (10), $\boldsymbol{q}_{m,k_p}^{res}$ is a virtual assignment to pilot tone in guard bands and will not be transmitted. However, it will be kept saved and known to the receiver for better channel estimation. The need for the residual sequence will be described in the following sections. The time-domain sequences can be derived using IFFT by substituting (7) and (10) into (2) as,

$$\begin{aligned} \hat{p}_m^{per}[n] &= \sum_{k=0}^{N-1} q_m^{per}[k]\, e^{j2\pi nk/N}, \\ \hat{p}_m^{aper}[n] &= \sum_{k=0}^{N-1} q_m^{aper}[k]\, e^{j2\pi nk/N}, \\ \hat{p}_m^{res}[n] &= \sum_{k=0}^{N-1} q_m^{res}[k]\, e^{j2\pi nk/N}, \quad \text{and} \\ \hat{p}_m^{per}[n] &= \hat{p}_m^{aper}[n] + \hat{p}_m^{res}[n]. \end{aligned} \tag{11}$$

where $\hat{p}_{[\cdot]}^{[\cdot]}[n]$ is the time-domain representation of $q_{[\cdot]}^{[\cdot]}[k]$. The sequence $\hat{p}_m^{per}[n]$ is a perfect periodic sequence and has an impulse like cyclic autocorrelation (AC) function defined as,

$$R_{\hat{p}\hat{p}}[n] = R_{\hat{p}\hat{p}}[0]\,\delta[n], \tag{12}$$

where

$$\delta[n] \overset{\text{def}}{=} \begin{cases} 1, & n = 0; \\ 0, & n \neq 0. \end{cases} \tag{13}$$

is the unit impulse function. Similarly, the AC function of SC or aperiodic sequence, $\hat{p}_m^{aper}[n]$, can be written as,

$$R_{\hat{p}\hat{p}}^{aper}[n] = \sum_{\ell=0}^{N-1} \hat{p}_m^{aper}[\ell]\, \hat{p}_m^{aper*}\left[(\ell - n)_{\text{mod } N}\right], \tag{14}$$

where the asterisk $(*)$ in superscript denotes complex conjugate. The zero-lag component of $R_{\hat{p}\hat{p}}^{aper}(n)$ will have the highest energy and can be written as,

$$R_{\hat{p}\hat{p}}^{aper}[n] = \begin{cases} R_{\hat{p}\hat{p}}^{aper}[0], & n = 0, \\ \tilde{R}_{\hat{p}\hat{p}}^{aper}[n], & n \neq 0, \end{cases} \tag{15}$$

where

$$\tilde{R}_{\hat{p}\hat{p}}^{aper}[n] = \sum_{\substack{\ell=0 \\ n\neq 0}}^{N-1} \hat{p}_m^{aper}[\ell]\, \hat{p}_m^{aper*}\left[(\ell - n)_{\text{mod}N}\right]. \tag{16}$$

Note that $\tilde{R}_{\hat{p}\hat{p}}^{aper}[n]$ is the cyclic correlation error term due to imperfect sequence. The AC of $\hat{p}_m^{res}[n]$ can be computed in the similar way and it will also contain a cyclic correlation error. The cyclic AC function for $\hat{p}_m^{per}[n]$ can be written as,

$$\begin{aligned} R_{m,\hat{p}\hat{p}}^{per}[n] &= \left(\hat{p}_m^{aper}[n] + \hat{p}_m^{res}[n]\right) \otimes \left(\hat{p}_m^{aper}[n] + \hat{p}_m^{res}[n]\right) \\ &= R_{m,\hat{p}\hat{p}}^{aper}[n] + R_{m,\hat{p}\hat{p}}^{res}[n]. \end{aligned} \tag{17}$$

In the above equation, the cyclic cross-correlation (CC) between aperiodic and residual sequences will result in zero because both sequences are orthogonal to each other. Let's consider an example of $N = 64$ subcarrier spectrally constrained OFDM system. The AC and CC output of the example presented above is illustrated in Figure 2. Figure 2 (a) represents the amplitude of AC of an aperiodic sequence, and Figure 2 (b) shows the amplitude of the AC of residual sequence. The CC of aperiodic and residual sequence is presented in Figure 2 (c). It can be observed that both sequences are orthogonal to each other. Figure 2 (d) depicts the AC of periodic sequence.

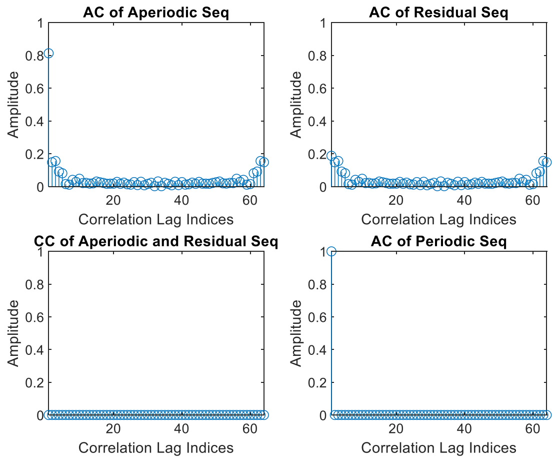


**FIGURE 2.** OFDM system with all subcarrier occupied by Pilot Sequence, (a) AC function of aperiodic sequence, (b) AC function of residual sequence, (c) CC between aperiodic and residual sequence, (d) AC of perfect periodic sequence.

## III. CHANNEL IMPULSE RESPONSE ESTIMATION

The impulse response of the multipath channel for an ideal unit impulse or delta function, $\delta[n]$, can be given as,

$$\begin{aligned} h[n] &= \sum_{l=0}^{L-1} \alpha_l e^{j\theta_l} \delta[n-\tau_l], \\ &= \sum_{l=0}^{L-1} h_l \delta[n-\tau_l], \end{aligned} \tag{18}$$

where $L$ is the total number of multipath, $\alpha_l$ is the amplitude, $\tau_l$ is an additional time delay and $\theta_l = 2\pi f_c \tau_l$ is the phase associated with the $l^{th}$ path. The transmitted signal, $x_m[n]$, passes through the multipath channel, producing a received baseband signal, $y_m[n]$, for $m$th symbol can be written as,

$$\begin{aligned} y_m[n] &= \sum_{l=0}^{L-1} h_{m,l} x_m[n-\tau_l] + w_m[n], \quad \text{or} \\ y_m[n] &= h_m[n] * x_m[n] + w_m[n], \end{aligned} \tag{19}$$

where $w[n]$ is additive white Gaussian noise (AWGN). As the cyclic prefix OFDM system is related to cyclic convolution between the channel and the OFDM symbols, (19) can be written as,

$$y_m[n] = h_m[n] \circledast x_m[n] + w_m[n], \tag{20}$$

where the operator $\circledast$ represents cyclic convolution.

### A. TIME-DOMAIN CHANNEL ESTIMATION: WITHOUT GUARD AND NULL SUBCARRIERS

The transmitted signal using (2), (10) and (11) can be written as,

$$x_m[n] = \hat{p}_m^{per}[n] = \sum_{k=0}^{N-1} q_m[n] e^{j2\pi nk/N}. \tag{21}$$

The discrete samples of the received baseband signal in time-domain can be written as,

$$y_m[n] = h_m[n] \circledast \hat{p}_m^{per}[n] + w_m[n], \tag{22}$$

where, $n = 0, 1, 2, \ldots, N-1$. The most straight forward way to estimate the CIR is to cross-correlate a known pilot sequence with the received waveform as,

$$R_{m,y\hat{p}}[n] = h_m[n] \circledast R_{m,\hat{p}\hat{p}}[n] + R_{m,w\hat{p}}[n], \tag{23}$$

where $R_{y\hat{p}}[n]$ is the cross-correlation between received signal, $y[n]$, and pilot sequence, $\hat{p}_m^{per}[n]$ and $R_{w\hat{p}}[n]$ is the cross-correlation between noise, $w[n]$, and the pilot sequence $\hat{p}_m^{per}[n]$. For a single-tap channel, the cross-correlation function can be written as,

$$R_{m,y\hat{p}}[n] = h_m[n] \circledast R_{m,\hat{p}\hat{p}}[0]\,\delta[n] + R_{m,w\hat{p}}[n], \tag{24}$$

or

$$R_{m,y\hat{p}}[n] = \tilde{h}_m[n] = h_m[n] + R_{m,w\hat{p}}[n], \tag{25}$$

where, $\tilde{h}[n]$ is the estimated CIR. The noise correlation term, $R_{w\hat{p}}[n]$, is added to the $h[n]$ and it is the major error term in the estimation for a perfect periodic sequence. For higher signal to noise (SNR) scenarios, $R_{w\hat{p}}[n] \rightarrow 0$ then the estimated CIR, $\tilde{h}[n] \cong h[n]$.

### B. TIME-DOMAIN CHANNEL ESTIMATION: WITH GUARD AND NULL SUBCARRIERS

In a practical OFDM system, guard bands are introduced on the upper and lower side of the spectrum to avoid adjacent channel interference (ACI). Due to the added guard and null sub-carriers, the periodicity of the pilots cannot be maintained, and the cyclic AC function does not result in a delta function. The AC side lobes, appearing in a spectrally constrained system, cause severe degradation in the performance of both frequency-domain and time-domain channel estimation techniques. In noisy multipath channel scenarios, the superposition of sides lobes and multipath taps creates additional ambiguity in detecting low energy taps correctly.

Then the cross-correlation of known pilot sequence with the received waveform is given as,

$$R_{m,y\hat{p}}[n] = h_m[n] \circledast R_{m,\hat{p}\hat{p}}^{aper}[n] + R_{m,w\hat{p}}[n] \tag{26}$$

where $R_{y\hat{p}}[n]$ is the cross-correlation between received signal, $y[n]$, and pilot sequence, $\hat{p}_m^{aper}[n]$, and $R_{w\hat{p}}[n]$ is the cross-correlation between noise, $w[n]$, and the pilot sequence $\hat{p}_m^{aper}[n]$. Assuming a quasi-static channel, (26) for multipath CIR can be written as,

$$R_{m,y\hat{p}}[n] = \sum_{l=0}^{L-1} h_{m,l} R_{m,\hat{p}\hat{p}}^{aper}\left[(n-\tau_l)_{\mathrm{mod}N}\right] + R_{m,w\hat{p}}[n], \tag{27}$$

$$R_{m,\hat{p}\hat{p}}^{aper}[n-\tau_l]_{\mathrm{mod}N} = \begin{cases} R_{m,\hat{p}\hat{p}}^{aper}[0], & n=\tau_l \\ \tilde{R}_{m,\hat{p}\hat{p}}^{aper}\left[(n-\tau_l)_{\mathrm{mod}N}\right], & n \neq \tau_l. \end{cases} \tag{28}$$

Equation (26), can be written as,

$$R_{m,y\hat{p}}[n] = \tilde{h}_m[n] = \begin{cases} \sum_{l=0}^{L-1} h_{m,l} R_{m,\hat{p}\hat{p}}^{aper}[0] + R_{m,w\hat{p}}[0], & n=\tau_l \\ R_{m,err}[n] + R_{m,w\hat{p}}[n], & n \neq \tau_l \end{cases} \tag{29}$$

where,

$$R_{m,err}[n] = \sum_{\substack{l=0 \\ n\neq\tau_l}}^{L-1} h_{m,l} \tilde{R}_{m,\hat{p}\hat{p}}^{aper}\left[(n-\tau_l)_{\mathrm{mod}N}\right]. \tag{30}$$

In the above equation, the estimated CIR, $\tilde{h}[n]$, has two sources of errors. One is the noise correlation term, $R_{w\hat{p}}[n]$, and the other is the cyclic correlation error (CCE) due to imperfect sequence. Since $R_{m,\hat{p}\hat{p}}^{aper}[0]$ contains the maximum correlation energy, the high energy taps can be easily detected. However, low energy taps may be suppress the side-lobes and result in higher estimation errors. For flat fading channel, the CCE can be reduced by

$$\begin{aligned} \tilde{h}_m[n] &= R_{m,y\hat{p}}[n] - R_{m,err}[n], \\ &= h_{m,l} R_{m,\hat{p}\hat{p}}^{aper}[0] + R_{m,w\hat{p}}[n] \end{aligned} \tag{31}$$

However, for the multipath fading channel, iterative algorithms are required to remove the CCE.

It's worth noting that, in the OFDM data communication system, only a few pilots are used for training purpose, and a perfect sequence is upsampled to assign values to the pilot tones to keep the periodicity. The AC function will have a sub-period that depends on the number of pilot tones, $N_p$. The sub-period $N_p$ defines the maximum length of CIR. Hence, $N_p$ must be greater than or equal to the length of a cyclic prefix for time-domain techniques.

## IV. PROPOSED SPECTRALLY CONSTRAINED TIME-DOMAIN (SCTD) CHANNEL ESTIMATION

Due to CCE, the deconvolution of the CIR from data becomes a challenging task for spectrally constrained waveforms. Therefore, in this work, a novel approach is used to fulfill the periodicity requirement by combining two aperiodic sequences extracted from one periodic sequence. The seed sequence meets the zero-correlation requirement. However, the primary aperiodic sequence is designed to meet the spectrum shaping. The remaining sequence or residual sequence is saved for further processing at the receiver side. The definition of aperiodic and residual sequences is presented in Section II. As shown in (17), aperiodic, and residual sequences are orthogonal to each other, and the summation of both sequences leads to a perfect periodic sequence. The advantage of the proposed scheme is that side lobes can be reduced significantly by fulfilling the periodicity requirement. The performance of the estimation of the channel transfer function at the receiver can be achieved with a simple iterative process with very low complexity. The architecture of the proposed OFDM system is shown in Figure 3.

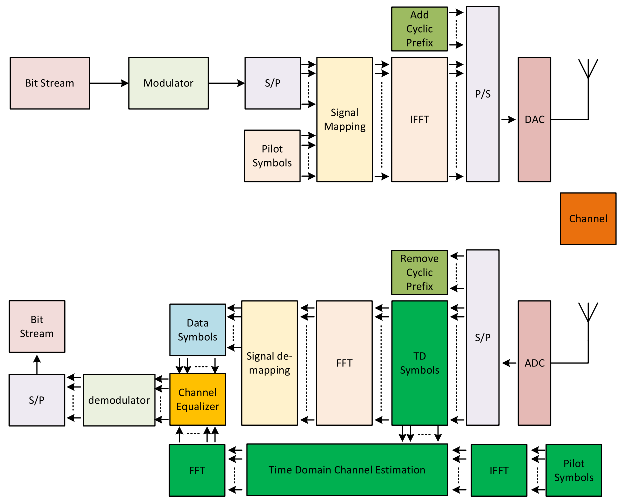


**FIGURE 3. Proposed baseband transceiver OFDM system model.**

For the perfect periodic sequence case, the discrete samples of the received baseband signal in the time-domain from (22) can be written as

$$y_m[n] = h_m[n] \circledast \left(\hat{p}_m^{aper}[n] + \hat{p}_m^{res}[n]\right) + w_m[n], \tag{32}$$

and the CC of the received signal with $\hat{p}_m^{per}[n]$ results in

$$R_{m,y\hat{p}}[n] = h_m[n] \circledast \left(R_{m,\hat{p}\hat{p}}^{aper}[n] + R_{m,\hat{p}\hat{p}}^{res}[n]\right) + R_{m,w\hat{p}}[n] \tag{33}$$

The estimated CIR can be obtained as,

$$\begin{aligned} R_{m,y\hat{p}}[n] &= \tilde{h}_m[n] \\ &= h_m[n] \circledast \left(R_{m,\hat{p}\hat{p}}^{aper}[0] + R_{m,\hat{p}\hat{p}}^{res}[0]\right)\delta[n] \\ &\quad + R_{m,w\hat{p}}[n], \end{aligned} \tag{34}$$

which will result in

$$\tilde{h}_m[n] = h_m[n] + R_{m,w\hat{p}}[n]. \tag{35}$$

### A. CASE-1: CIR ESTIMATION FOR A FLAT FADING CHANNEL

For a flat fading SC-OFDM case, let's assume that pilot tones occupy all available subcarriers. The cyclic cross-correlation of the aperiodic sequence, $\hat{p}_m^{aper}[n]$, with the received waveform is given as,

$$R_{m,y\hat{p}}[n] = h_m[n] \circledast R_{m,\hat{p}\hat{p}}^{aper}[n] + R_{m,w\hat{p}}[n] \tag{36}$$

The estimated CIR for an aperiodic case is defined in (29). As previously described in the previous section, the CCE term is caused by an imperfect sequence. In this work, it is proposed to remove the CCE by completing the periodic sequence as defined in (11). The sum of $R_{m,\hat{p}\hat{p}}^{aper}[n]$ and $R_{m,\hat{p}\hat{p}}^{res}[n]$ will result in a perfect periodic sequence, and side lobes can be reduced significantly. For a flat fading channel, equation (29) can be written as,

$$\tilde{h}_m[n] = \begin{cases} h_{m,0}R_{m,\hat{p}\hat{p}}^{aper}[0] + +R_{m,w\hat{p}}[0], & n = \tau_l \\ R_{m,err}^{aper}[n] + R_{m,w\hat{p}}[n], & n \neq \tau_l \end{cases} \tag{37}$$

Since $h_{m,0}R_{m,\hat{p}\hat{p}}^{aper}[0] + R_{m,w\hat{p}}[0]$ is the significant channel tap, the first CIR estimate can be provided as,

$$\tilde{h}_m^{(1)}[n] = h_{m,0}R_{m,\hat{p}\hat{p}}^{aper}[0] + R_{m,w\hat{p}}[0] \tag{38}$$

The convolution of $\tilde{h}_m^{(1)}[n]$ with $R_{m,\hat{p}\hat{p}}^{res}[n]$ will result in

$$C_{m,\tilde{h}\circledast\hat{p}\hat{p}}^{res}[n] = \tilde{h}_m^{(1)}[n] \circledast R_{m,\hat{p}\hat{p}}^{res}[n], \tag{39}$$

or

$$C_{m,\tilde{h}\circledast\hat{p}\hat{p}}^{res}[n] = \begin{cases} \tilde{h}_{m,0}^{(1)}R_{m,\hat{p}\hat{p}}^{res}[0], & n = \tau_l \\ R_{m,err}^{res}[n], & n \neq \tau_l \end{cases} \tag{40}$$

The residual sequence completes the periodic sequence and the CCE term $R_{m,err}^{aper}[n] + R_{m,err}^{res}[n] = \varepsilon_m \to 0$, and $\tilde{h}_{m,0}^{(1)} \to h_{m,0}$. Thus, (29) can be written as,

$$\tilde{h}_m^{(2)}[n] = \begin{cases} h_{m,0}R_{m,\hat{p}\hat{p}}^{aper}[0] + \tilde{h}_{m,0}^{(1)}R_{m,\hat{p}\hat{p}}^{res}[0] \\ \quad + R_{m,w\hat{p}}[0], \quad n = \tau_l \\ \varepsilon_m + R_{m,w\hat{p}}[n], \quad n \neq \tau_l \end{cases} \tag{41}$$

In an ideal case where CIR estimation $\tilde{h}_{m,0}^{(1)} = h_{m,0}$ and $\varepsilon_m = 0$,

$$\tilde{h}_m^{(2)}[n] = h_{m,0}\delta[n] + R_{m,w\hat{p}}[n] \tag{42}$$

In the above equation, the CCE term is suppressed, and only the noise is the source of error in CIR estimation. However, in a practical system, $\tilde{h}_{m,0}^{(1)} \cong h_{m,0}$ and there will be a small residual error left in the estimation. The residual error can be further suppressed by employing an advanced noise level thresholding technique.

### B. CASE-2: CIR ESTIMATION FOR A MULTIPATH FADING CHANNEL

For the multipath fading channel, CCE cancellation requires an iterative procedure. The $i^{\text{th}}$ CIR can be estimated as,

$$\tilde{h}_m^i[n] = h_m[n] \circledast R_{m,\hat{p}\hat{p}}^{aper}[n] + R_{m,w\hat{p}}[n] \tag{43}$$

or

$$\tilde{h}_m^i[n] = \begin{cases} \sum_{l=0}^{L-1} h_{m,l}R_{m,\hat{p}\hat{p}}^{aper}[0] + R_{m,w\hat{p}}[0], & n = \tau_l \\ R_{m,err}^{aper}[n] + R_{m,w\hat{p}}[n], & n \neq \tau_l \end{cases} \tag{44}$$

Since channel length is finite and only a few taps contain significant energy, the CCE contributed from those channel taps will also be higher. Some of the low-energy channel taps might be suppressed in CCE and, due to noise, cannot be identified in the first iteration. For the first step, select the maximum energy path from the CIR as,

$$\check{h}_m^i[\tau_{l_{max}}] = h_{m,l_{max}}R_{m,\hat{p}\hat{p}}^{aper}[0] + R_{m,w\hat{p}}[\tau_{l_{max}}], \tag{45}$$

where $\check{h}_m^i$ is the first CIR estimate. The convolution of $\check{h}_m^i[\tau_{l_{max}}]$ with $R_{m,\hat{p}\hat{p}}^{res}[n]$ will result in

$$C_{m,\tilde{h}\circledast\hat{p}\hat{p}}^{res}[n] = \check{h}_m^i[\tau_{l_{max}}] \circledast R_{m,\hat{p}\hat{p}}^{res}[n], \tag{46}$$

or

$$C_{m,\tilde{h}\circledast\hat{p}\hat{p}}^{res}[n] = \begin{cases} \check{h}_{m,l_{max}}^i R_{m,\hat{p}\hat{p}}^{res}[0], & n = \tau_{l_{max}} \\ R_{m,err}^{res}[n], & n \neq \tau_{l_{max}} \end{cases} \tag{47}$$

The residual sequence completes the periodic sequence for the path $l_{max}$ and the CCE term $R_{m,err}^{aper}[n] + R_{m,err}^{res}[n] = \varepsilon_m \to 0$, and $\tilde{h}_m^i[n] \to h_m[n]$. By adding the correction term $C_{m,\tilde{h}\circledast\hat{p}\hat{p}}^{res}[n]$ to (44), the resultant CIR can be estimated as,

$$\tilde{h}_m^{i+1}[n] = \tilde{h}_m^i[n] + C_{m,\tilde{h}\circledast\hat{p}\hat{p}}^{res}[n] \tag{48}$$

$$\tilde{h}_m^{i+1}[n] = \begin{cases} \sum_{l=0}^{L-1} h_{m,l}R_{m,\hat{p}\hat{p}}^{aper}[0] + \check{h}_{m,l_{max}}^i R_{m,\hat{p}\hat{p}}^{res}[0] \\ \quad + R_{m,w\hat{p}}[0], \quad n = \tau_l \\ \varepsilon_m + R_{m,w\hat{p}}[0], \quad n \neq \tau_l \end{cases} \tag{49}$$

By canceling the CCE from the major tap, the side lobes will be reduced significantly, and it will allow the detection of the low-energy taps. One way is to reduce the CCE by iterating over all detected multipath channel taps and repeating the procedure from (45) to (49). The proposed algorithm has the advantage of removing all detected taps' CCE at once. The general form of the algorithm can be written as,

$$\tilde{h}_m^{i+1}[n] = \begin{cases} \sum_{l=0}^{L-1} h_{m,l}R_{m,\hat{p}\hat{p}}^{aper}[0] + \sum_{l=0}^{L-1} \tilde{h}_{m,l}^i R_{m,\hat{p}\hat{p}}^{res}[0] \\ \quad + R_{m,w\hat{p}}[0], \quad n = \tau_l \\ \varepsilon_m + R_{m,w\hat{p}}[0], \quad n \neq \tau_l \end{cases} \tag{50}$$

The error in each iteration can be computed as,

$$\epsilon_m^i = \sum_{n=0}^{L-1} \left| \tilde{h}_m^{i+1}[n] - \tilde{h}_m^i[n] \right|^2, \tag{51}$$

and the iterative procedure should meet the following condition,

$$\epsilon_m^{i-1} < \epsilon_m^i. \tag{52}$$

From (50) it can be observed that $\tilde{h}_m^i[n] \rightarrow h_m[n]$, and $\varepsilon_m \rightarrow 0$, the estimated CIR is

$$\tilde{h}_m^{i+1}[n] = h_m[n] + R_{m,w\hat{p}}[n]. \tag{53}$$

The above equation provides a CIR estimation in a noisy channel. The noise can be suppressed by defining a threshold $\gamma$ and removing the insignificant channel taps. The threshold $\gamma$ can be obtained from noise variance $\tilde{\sigma}^2$, and the final estimated CIR is given by

$$\tilde{h}_m^{i+1}[n] = \begin{cases} \tilde{h}_m^{i+1}[n], & \left|\tilde{h}_m^{i+1}[n]\right| \geq \gamma; \\ 0, & \text{otherwise.} \end{cases} \tag{54}$$

A similar procedure can be used for the upsampled pilot sequence case. However, the sub-period of cyclic auto- and cross-correlation will be equal to the length of the periodic pilot sequence, $N_p$, as described in previous sections.

So far, it is assumed that only the pilot sequence is transmitted. For the case of hybrid and data transmission modes, where data carriers are also present, the same derivation remains valid because there is no correlation between pilot and data tones.

### C. ALGORITHM FOR PROPOSED TIME-DOMAIN CHANNEL ESTIMATION

In the previous section, a new approach to time-domain channel estimation is presented. Briefly, the proposed time-domain technique provides an improved CIR by reducing CCE using an iterative procedure. The procedure starts with a time-domain correlation of spectrally constrained received waveform with a known training sequence. Then the CCE is canceled by fulfilling a perfect periodic condition. An overall overview of the proposed TD CIR estimation is illustrated in Figure 4. The steps used for the proposed TD CIR estimation are as follows:

1. Find the $i^{\text{th}}$ CIR estimate using the cyclic CC between discrete received waveform and known aperiodic pilot sequence using (44).
2. Calculate the power of estimated channel taps and select the maximum energy paths as given in (45). When $i = 0$, only one maximum energy path can be selected, however for $i > 0$ all detected paths can be selected at once.
3. Perform the cyclic convolution between residual sequence and channel path selected in step-2 using (46). This step can be efficiently conducted in the FFT domain efficiently.
4. Cancel the CCE caused by the maximum energy path using (49) by adding the outcome of (46) to (44) and obtain the $i + 1$ CIR estimate.
5. Calculate the error using (51). If the error meets the condition given in (52), return to step-2.
6. If CIR convergence criteria is met and CIR output is required, the algorithm gives an output for computed CIR, otherwise proceed with the next step.
7. If data is transmitted, then proceed with the channel equalization step; otherwise, terminate the algorithm.

### D. COMPUTATIONAL COMPLEXITY OF PROPOSED ALGORITHM

The number of complex multiplications needed to obtain the CIR comes from three main steps given in (44), (46), and (49). Equation (44) provides a cross-correlation between time-domain samples from received signal and spectrally constrained pilot sequence. Both have length equal to the FFT size, $N$. The general computational complexity of correlation is $O\left(N^2\right)$ in time domain. However, by using FFT the complexity can be reduced to $O(N \log N)$. The next step is the convolution and in the FFT domain the complexity is $O(N \log N)$. Equation (49) is an N-point addition operation. The total complexity of proposed algorithm is $O(N \log N)$ which is less than the computation complexity of conventional LS method $O\left(N^3\right)$.

## V. MULTIBAND CIR ESTIMATION

As described in Section II, a UWB is divided into $S$ multiband to meet the hardware BW specifications. At the receiver, CIR is estimated using the proposed time-domain method for each subband, and $FFT$ is used to compute the CTF. The CTF for $s$ subband during $m$th time duration can be written as,

$$\tilde{H}_{m,s}[k] = H_{m,s}[k] + \breve{R}_{m,w\hat{p}}[k] \tag{55}$$

where $s = 1, 2, \ldots, S$, $\breve{R}_{m,w\hat{p}}[k] = FFT(R_{m,w\hat{p}}[n])$, and $S$ is the total number of multiband.

The MB CTF is obtained by concatenating the CTF of each subband as,

$$\tilde{H}_{m,\text{mb}}[k_{\text{mb}}] = \left[\tilde{H}_{m,1}[k_1], \tilde{H}_{m,2}[k_2], \ldots, \tilde{H}_{m,S}[k_S]\right] \tag{56}$$

where $k_s = 0, 1, 2, \ldots, N-1$, and $k_{\text{mb}} = [k_1, k_2, \ldots, k_S]_{SN\times 1}$. Finally, the MB CIR is obtained using $IFFT$ as,

$$\tilde{h}_{m,\text{mb}}[n_{\text{mb}}] = IFFT\left[\tilde{H}_{m,\text{mb}}[k_{\text{mb}}]\right] \tag{57}$$

In the above equation, high-resolution CIR is obtained. Since the sampling rate for each band is the same, the symbol duration will remain the same for the MB scenario.

## VI. RESULTS AND DISCUSSION

In this section, various numerical experiments are performed to validate the proposed MB channel sounders' post-processing techniques. The proposed technique, SCTD, is implemented in MATLAB. In this work, known CSI is used as a benchmark. We have also implemented conventional techniques such as LS, DFT-based, LS, and FPTC to evaluate the proposed TD techniques. Besides, the performance of newly developed time-domain CIR estimation techniques is examined in arbitrary spectral constrained conditions. Furthermore, the study is extended for data communication, and performance is evaluated against conventional methods.

The proposed estimation results are validated by comparing them with those of known CIR, theoretical, LS, LS-DFT, and FPTC. The testing performed here shows that the particular implementation of the proposed implementation of CIR estimation techniques is valid and suitable for their intended purpose within a reasonable bound of accuracy. MSE is computed for each case with known CIR as a reference for detailed performance evaluation. The channel transfer function, CTF is computed using the FFT of CIR, and the formula used to calculate MSE is given by [57],

$$MSE = E\left\{\left|H[k] - \tilde{H}[k]\right|^2\right\}, \tag{58}$$

where $H[k]$ is the known CTF and $\tilde{H}[k]$ is the estimated CTF using proposed and conventional techniques. An average MSE is computed using Monte Carlo simulation for different $E_b/N_0$ scenarios in various environmental conditions.

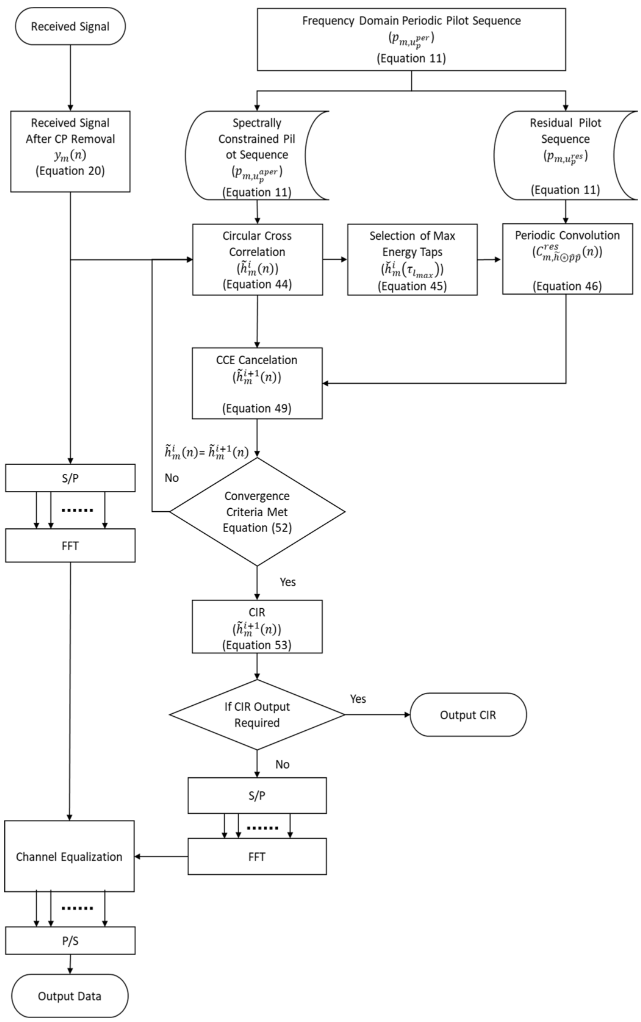


**FIGURE 4.** Algorithm illustration for the proposed time-domain channel estimation method.

**TABLE 1.** Simulation parameters for MB transmission in Rayleigh channel.

| System Parameters | | Value |
|---|---|---|
| Hybrid Mode | Number of Pilot subcarriers | 27 |
| | Number of Data subcarriers | 26 |
| Modulation Type | | QPSK |
| Sampling Rate (Msps) | | 20 |
| Number of guard subcarriers | | 10 |
| $\Delta f$: subcarrier spacing (kHz) | | 312.5 |
| $T_b$: OFDM Symbol duration of subband ($\mu$sec) | | 3.2 |
| $T_c$: Cyclic Prefix duration of subband ($\mu$sec) | | 1.6 |
| $T_g$: Guard Interval duration ($\mu$sec) | | 0.25 |
| $T_{sym}$: Symbol duration ($\mu$sec) | | 5.05 |
| Number of multiband | | 10 |
| Number of transmitters | | 2 |

## A. DISCUSSION ON THE NUMBER OF ITERATIONS FOR THE PROPOSED SCTD TECHNIQUE

The first step is to identify the number of iterations required to achieve the desired accuracy for the proposed iterative post-processing technique. The MATLAB implementation of the proposed sounder design supports a highly flexible MB architecture. However, the cost-effective SDR offers a minimal baseband bandwidth in the range of 20 MHz. These hardware constraints are taken into account while demonstrating the performance of the proposed sounder design. Transmission in the Rayleigh channel is considered to evaluate the performance of the proposed channel sounder.

It is assumed that two coherent and independent transmitter resources are available—each transmitter supports a bandwidth of 20 MHz of the system bandwidth. An MB bandwidth of 200 MHz is considered. The total number of multiband is 10. A unique time-frequency code is used for each transmitter. Transmitter one is assigned code $\{1, 3, 5, 7, 9\}$, and transmitter two has the code $\{2, 4, 6, 8, 10\}$. A resource mapping of MB switching is shown in Figure 5. Since we have two transmitter resources available, the total number of switching time slots is 5. Switching between two bands has a guard duration. The system configurations of the SC hybrid mode are used for the simulation. The FFT length of 64-point is used for each subband, and a cyclic prefix of 1/2 of FFT-size is used. The symbol duration without cyclic prefix and guard period is 3.2 $\mu$sec. The 4-QAM data modulation order is used. The MSE results are compared with those from theoretical and conventional techniques. The summary of simulation parameters is given in Table 1.

### 1) TRANSMISSION IN FREQUENCY SELECTIVE CHANNEL

The first numerical experiment is performed in the frequency-selective stationary Rayleigh channel. The power

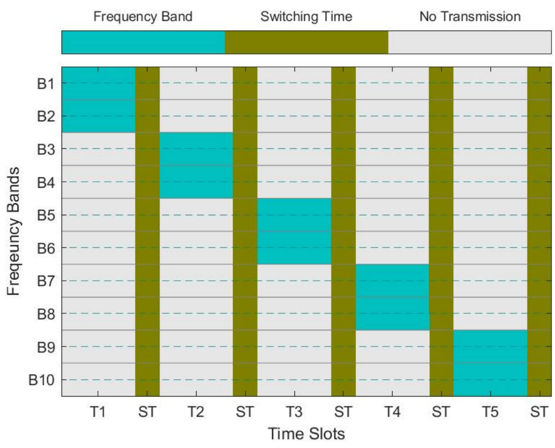


**FIGURE 5.** Resource mapping of MB-OFDM sounder.

**TABLE 2.** Power delay profile for a frequency selective Rayleigh channel.

| Path No. | Delay (μs) | Power (dB) |
|---|---|---|
| 1 | 0 | -3 |
| 2 | 0.0020 | -9 |
| 3 | 0.0100 | -3 |
| 4 | 0.0500 | -6 |
| 5 | 0.2000 | -9 |
| 6 | 0.3000 | -12 |

delay profile of the 6-tap channel is described in Table 2.

Figure 6 shows the semi-logarithmic plot of MSE results from Monte Carlo simulations for $E_b/N_0$ values ranging from 0 until 30 dB. The results compare LS, LS-DFT, FPTC, and SCTD at different iteration levels. It can be observed that the proposed SCTD technique shows improved performance for low $E_b/N_0$ cases. The 2$^{nd}$ and 5$^{th}$ iteration of SCTD provides a significant improvement for less than 15 dB $E_b/N_0$ and offers more than 3dB advantage for similar MSE values as compared to conventional techniques. For higher $E_b/N_0$ values, the 1$^{st}$, 2$^{nd}$, and 5$^{th}$ iterations of SCTD did not perform well compared to traditional methods. We further tested the convergence of SCTD at a higher number of iterations. At the 10$^{th}$ Iteration, SCTD supersedes all conventional methods and provides a significant advantage for the same MSE value. In other words, for a fixed threshold of MSE at $10^{-3}$ LS and FPTC require 17 dB of $E_b/N_0$ while SCTD can reach the performance threshold at 12 dB, which is a significant improvement against conventional techniques. It will be safe to conclude that the proposed SCTD technique converges to a solution and provide superior results within ten steps of iterations.

As explained in the experiment setup above, hybrid system configurations are used to evaluate the SCTD performance. Since data is also transmitted on approximately 50% of available subcarriers, Figure 7 shows the comparison of BER results from LS, LS-DFT, FPTC, and SCTD at different iteration levels. A zoomed-in plot of BER for 15 to 21 dB of $E_b/N_0$ is also provided for detailed comparison and insight. As we have discussed, the MSE of SCTD at 1$^{st}$ and 2$^{nd}$ iteration only performs better for lower $E_b/N_0$ values. It is also apparent from the results that BER is higher for SCTD at the 1$^{st}$, 2$^{nd}$, 5$^{th}$ iteration as compared to other techniques for high $E_b/N_0$ values. However, SCTD at the 10$^{th}$ iteration results supersedes conventional methods. For a fixed BER threshold, SCTD provides an average of 3 dB improvement in the frequency selective Rayleigh channel environment.

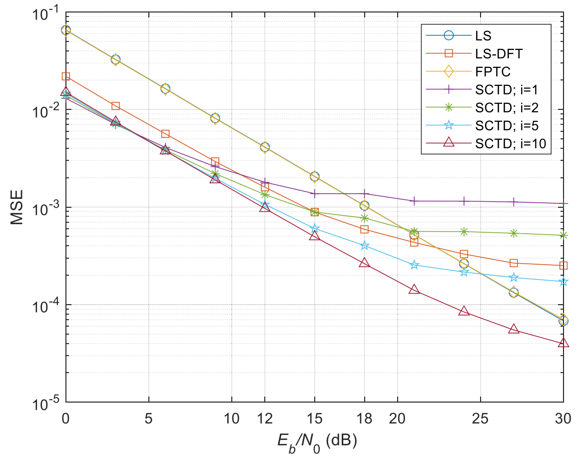


**FIGURE 6.** Comparison of MSE performance between conventional techniques and SCTD for frequency-selective Rayleigh channel without doppler.

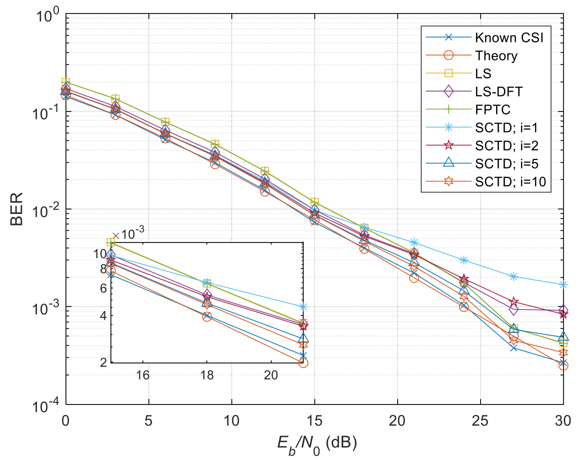


**FIGURE 7.** Comparison of BER performance between conventional techniques and SCTD for frequency-selective Rayleigh channel without doppler.

For further study, a comparison of an instantaneous CIR from simulations is presented for a 30 dB $E_b/N_0$ in Figure 8. The $x$-axis represents the time from 0 to 1 $\mu$sec and $y$-axis represents the linear gain of each channel tap. As described in the simulation setup, we have assumed six tap Rayleigh channels to evaluate the proposed technique's performance. Since SC waveform results in high sides lobes, these sides lobes can be observed for conventional methods in Figure 8. To provide a detailed insight into the estimated CIR using

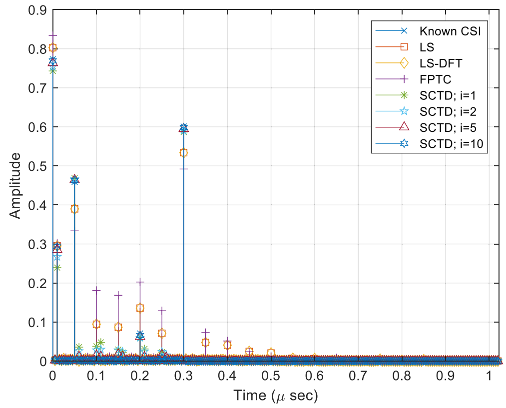


**FIGURE 8.** Comparison of CIR performance between conventional techniques and SCTD for frequency-selective Rayleigh channel without doppler.

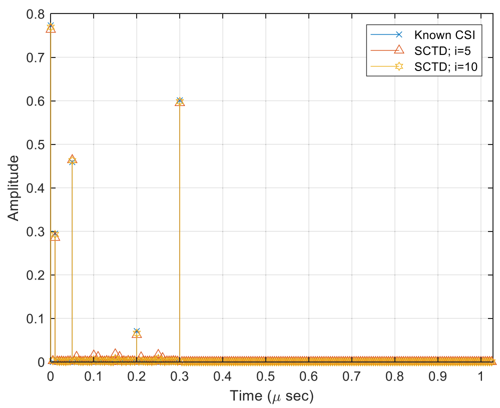


**FIGURE 9.** Comparison of instantaneous CIR between known CSI and SCTD for frequency-selective Rayleigh channel without doppler.

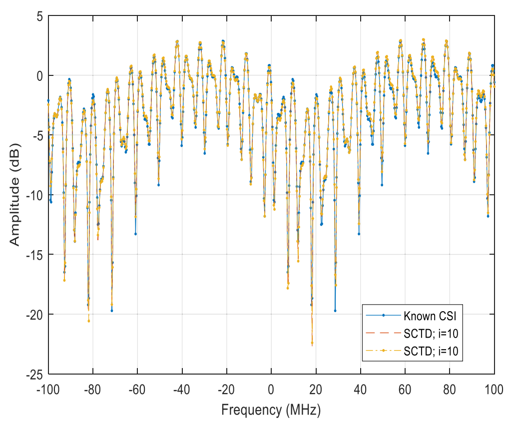


**FIGURE 10.** Comparison of instantaneous CTF between known CSI and SCTD for frequency-selective Rayleigh channel without doppler

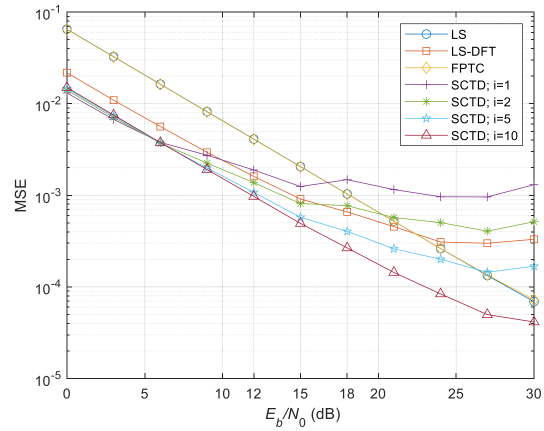


**FIGURE 11.** Comparison of MSE performance between conventional techniques and SCTD for mobile Rayleigh channel.

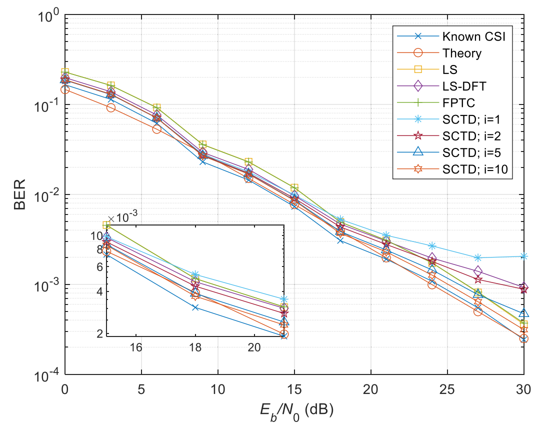


**FIGURE 12.** Comparison of BER performance between conventional techniques and SCTD for mobile Rayleigh channel.

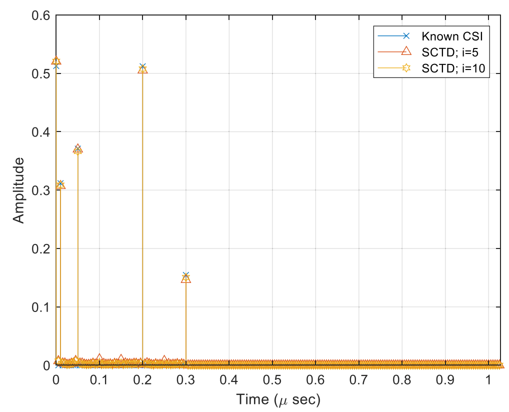


**FIGURE 13.** Comparison of instantaneous CIR between known CSI and SCTD for mobile Rayleigh channel.

proposed SCTD, the results from SCTD at the 5th and 10th iterations are compared with known CSI in Figure 9. It can be observed that even the smallest taps can be identified using the proposed SCTD method. Results show that SCTD with ten and more iterations provides the best performance, and residual error due to SC is reduced significantly for frequency selective channel. It should be noted that Figure 8 only demonstrates the residual error reduction for one instance. For the detailed MSE performance of the proposed algorithm, the reader may refer to Figure 6.

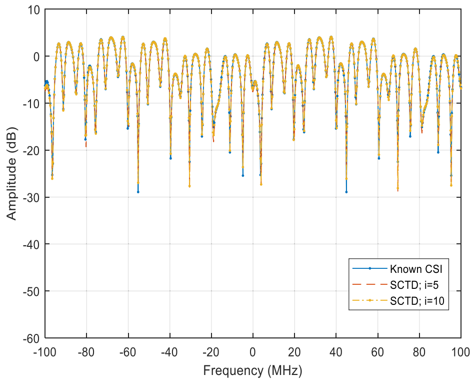


**FIGURE 14. Comparison of instantaneous CTF between known CSI and SCTD for mobile Rayleigh channel.**

Furthermore, the CTF is presented for 30 dB $E_b/N_0$ in Figure 10 to provide a detailed insight in the FD and a comparison of an instantaneous CTF between conventional techniques and SCTD at different iteration levels. The $x$-axis represents the 200 MHz frequency channel, and the $y$-axis provides channel gain in dB. The CTF of the known CSI case does not include the noise artifact. However, numerical experiments were performed with AWGN noise. Each subchannel is 20 MHz wide and has SC due to guard band and DC-subcarrier. From the results, a very good match can be observed between the known CSI and SCTD methods.

### 2) TRANSMISSION IN FREQUENCY SELECTIVE MOBILE CHANNEL

Another study is performed for a mobile channel. We used the same multipath frequency selective channel profile as in the previous section. However, in this case, it is considered that the receiver is moving at a velocity of 100 km/h. Figure 11 shows the semi-logarithmic plot of MSE results from Monte Carlo simulations for $E_b/N_0$ values from 0 until 30 dB. The results show that SCTD's excellent performance is almost similar to the stationary channel case. It can be observed that for a fixed threshold of MSE at $10^{-3}$, LS and FPTC require 17 dB of $E_b/N_0$ while SCTD can reach the threshold of performance at 12 dB, which is a significant improvement. Similarly, the BER performance of SCTD at the $10^{\text{th}}$ iteration supersedes all other methods, as shown in Figure 12. From these observations, it can be concluded that the proposed SCTD technique converges to a solution and provides superior results within ten iterations for mobile frequency selective channels as well.

For further study, a comparison of an instantaneous CIR and CTF are presented in Figure 13 and Figure 14, respectively. It can be seen that the proposed algorithm manages to reduce the correlation residual error and has the ability to detect smaller power taps. These results lead to better CTF estimation. In addition, the proposed algorithm does not suffer from interpolation error as presented in frequency domain channel estimation methods.

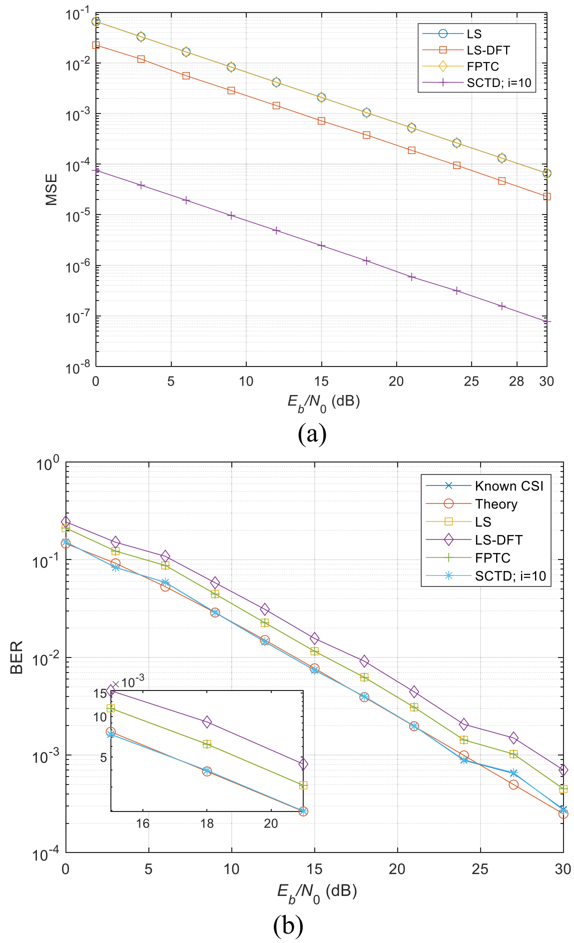


**FIGURE 15. Results for the pilot density of 50.4% (a) MSE (b) BER.**

## B. PERFORMANCE OF PROPOSED SCTD POST-PROCESSING TECHNIQUE WITH DIFFERENT PILOT DENSITY

Next, the study is performed to identify the number of pilots required to achieve the desired performance for the proposed iterative post-processing technique. A similar simulation setup described in the previous section is used for this study, but with the FFT length of 256-Point for each subband. The symbol duration without cyclic prefix and guard period is 12.8$\mu$sec. Various pilot density cases are discussed. The MSE results are compared with those from theoretical and conventional techniques. The performance of SCTD for frequency selective stationary Raleigh channels is presented here. In this experiment, a six-tap Rayleigh fading channel without a Doppler is considered in Table 2 to provide an additional channel condition, and the summary of additional simulation parameters is given in Table 3.

Figure 15, 16, 17, and 18 show the performance of the system with 50.4%, 25.6%, 12.8%, and 6.4% pilot density, respectively. The $x$-axis represents a range of $E_b/N_0$ from 0 to 30 dB, and the $y$-axis represents the logarithmic value of errors. Figure 15 (a) shows that for same pilot density, the

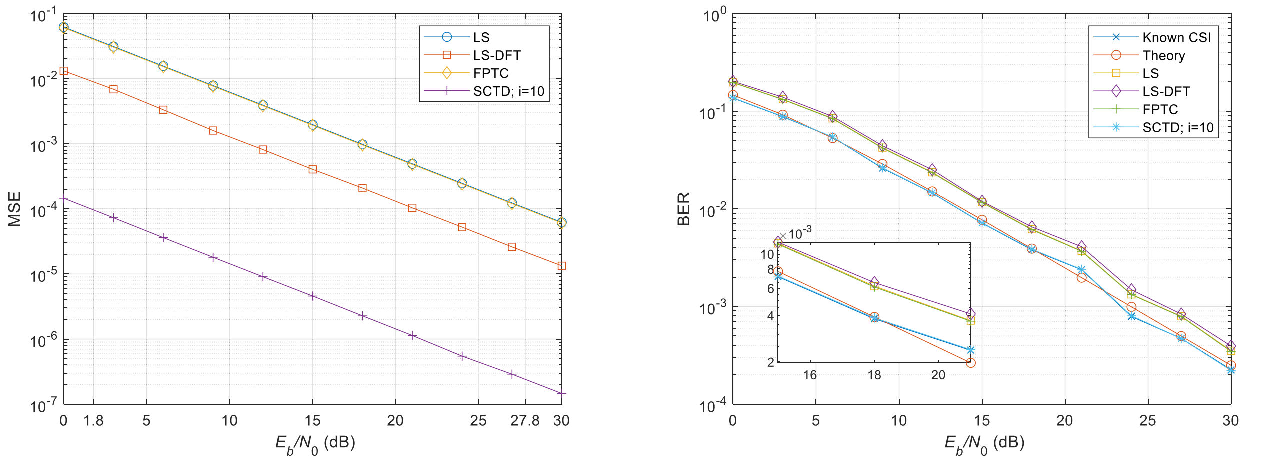


(a) (b)

**FIGURE 16.** Results for the pilot density of 25.6% (a) MSE (b) BER.

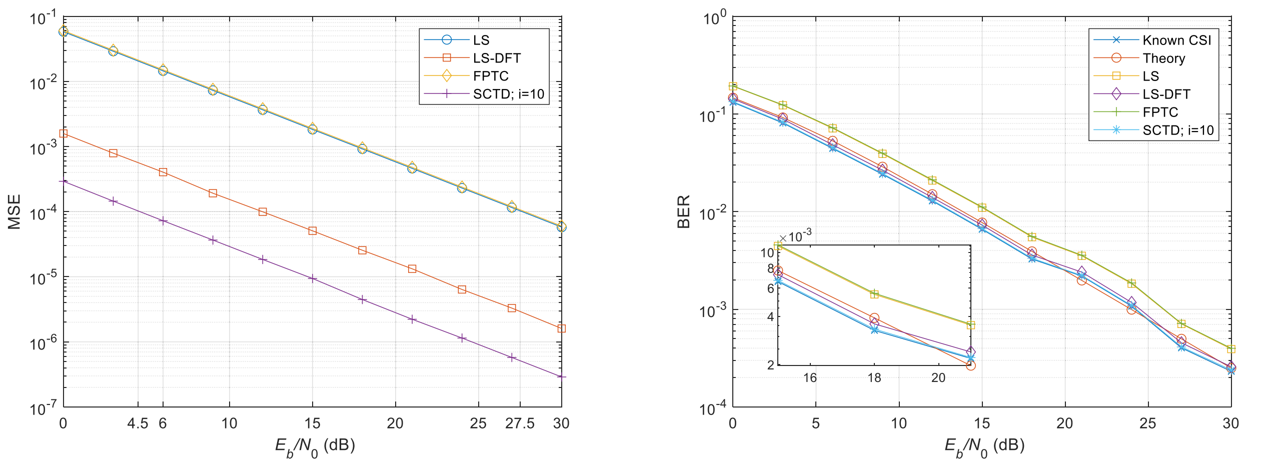


(a) (b)

**FIGURE 17.** Results for the pilot density of 12.8% (a) MSE (b) BER.

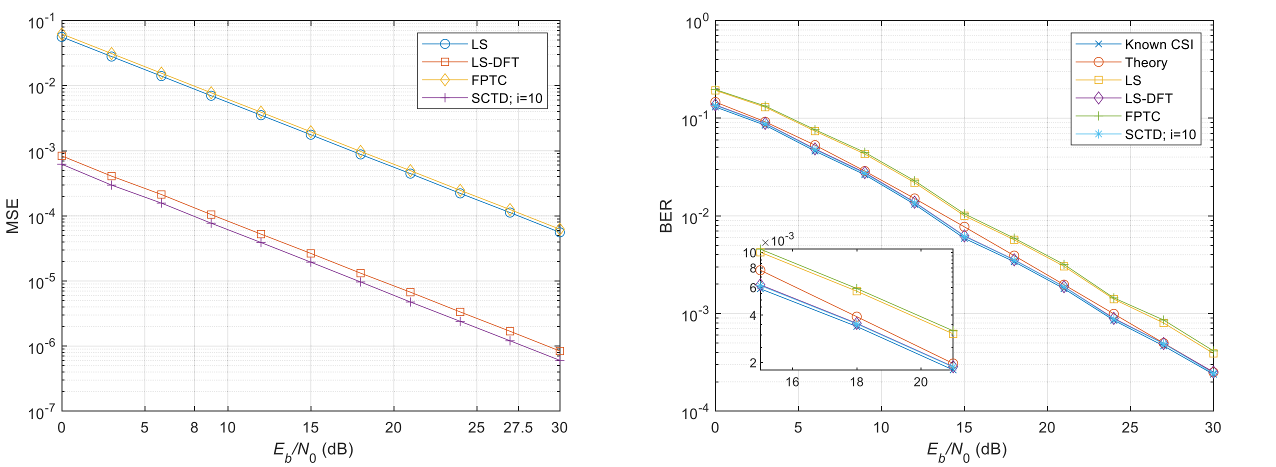


(a) (b)

**FIGURE 18.** Results for the pilot density of 6.4% (a) MSE (b) BER.

proposed SCTD outperforms all conventional techniques. For a fixed threshold of MSE at $10^{-3}$, the SCTD has over 20 dB of advantage over other methods. In other words, the proposed techniques require far less pilot density to meet similar MSE

**TABLE 3. Simulation parameters for MB-OFDM transmission in Rayleigh channel for pilot density analysis.**

<table>
<tr><th colspan="2">System Parameters</th><th colspan="4">Value</th></tr>
<tr><td rowspan="3">Hybrid Mode</td><td>Number of Pilot subcarriers</td><td>110</td><td>56</td><td>28</td><td>14</td></tr>
<tr><td>Number of Data subcarriers</td><td>108</td><td>162</td><td>190</td><td>204</td></tr>
<tr><td>Pilot Density (Percentage)</td><td>50.4%</td><td>25.6%</td><td>12.8%</td><td>6.4%</td></tr>
<tr><td colspan="2">Modulation Type</td><td colspan="4">QPSK</td></tr>
<tr><td colspan="2">Sampling Rate (Msps)</td><td colspan="4">20</td></tr>
<tr><td colspan="2">Number of guard subcarriers</td><td colspan="4">38</td></tr>
<tr><td colspan="2">$\Delta f$: subcarrier spacing (KHz)</td><td colspan="4">312.5</td></tr>
<tr><td colspan="2">$T_b$: OFDM Symbol duration of subband ($\mu$sec)</td><td colspan="4">12.8</td></tr>
<tr><td colspan="2">$T_c$: Cyclic Prefix duration of subband ($\mu$sec)</td><td colspan="4">6.4</td></tr>
<tr><td colspan="2">$T_g$: Guard Interval duration ($\mu$sec)</td><td colspan="4">0.25</td></tr>
<tr><td colspan="2">$T_{sym}$: Symbol duration ($\mu$sec)</td><td colspan="4">19.45</td></tr>
<tr><td colspan="2">Speed of mobile (km/h)</td><td colspan="4">-</td></tr>
<tr><td colspan="2">Number of multiband</td><td colspan="4">10</td></tr>
<tr><td colspan="2">No of transmitter</td><td colspan="4">2</td></tr>
<tr><td colspan="2">No of fading channel taps</td><td colspan="4">6</td></tr>
<tr><td colspan="2">No of Iteration for SCTD</td><td colspan="4">5</td></tr>
</table>

requirements. Figure 15 (b) shows the BER performance, and SCTD has a good match with theoretical performance. For further analysis, we have reduced the pilot density to half, and MSE and BER results are presented in Figure 16. Since the pilot density is higher than channel length, the performance of SCTD is at least 15 dB better than conventional techniques for the same MSE values. Two low pilot density cases are presented in Figure 17 and Figure 18. Even for a small number of pilots, the SCTD still has superior performance than conventional techniques. This shows that even though the proposed method is primarily designed for channel-sounding applications, it is still suitable for data communication applications. The results show that the SCTD technique requires fewer pilot tones, which also means that more data carriers are available for the system to transmit.

In summary, the first study is performed to evaluate the number of iterations required by the proposed SCTD technique to converge. It is found that a maximum of five iterations is required for a flat fading channel, and within ten iterations, the proposal solution supersedes the conventional technique for stationary and mobile frequency-selective channels. Another study is performed to compare the proposed SCTD scheme's performance with traditional methods with different pilot densities. It was observed that the proposed SCTD method requires fewer pilots to provide similar performance. From the results, it is evident that multi-band SCTD performed very well for sounding application and CIR can be estimated with very high confidence for both stationary and mobile channels.

This study is also extended for communication application and proved very useful. However, in this article, only the results from sounding related numerical experiments are presented. Two potential applications where, the proposed algorithm can prove useful are highly sparse cognitive and digital video broadcasting (DVB) transmission cases. Overall, the proposed method is highly suitable for low $E_b/N_0$ regimes, and it has a high potential to be utilized in communication systems.

## VII. CONCLUSION

In this work, we introduced a new time-domain CIR estimation algorithm for channel sounding. This work proposed using the CASAZ family sequence-based probing signal due to their attractive low PAPR properties. The proposed time-domain channel estimation reduces the residual error of correlation due to spectrum-constrained waveforms. The performance of the newly developed technique is evaluated using an extensive numerical experimental study. The MSE and BER are computed for various cases. The accuracy of the proposed scheme is measured against conventional techniques and also known channel conditions. The simulation results show that the proposed MB time-domain iterative method, SCTD, outperformed conventional techniques for various Rayleigh channel conditions with AWGN. Results show that within ten iterations, the proposed solution supersedes the conventional technique for stationary and mobile frequency-selective channels. Furthermore, it is observed that the proposed SCTD method requires fewer pilots to provide similar performance. Finally, it can be concluded that the proposed SCTD channel estimation is highly suitable for low $E_b/N_0$ regimes and can also be used for various communication systems.

## REFERENCES

[1] T. S. Rappaport, S. Sun, R. Mayzus, H. Zhao, Y. Azar, K. Wang, G. N. Wong, J. K. Schulz, M. Samimi, and F. Gutierrez, "Millimeter wave mobile communications for 5G cellular: It will work!" *IEEE Access*, vol. 1, pp. 335–349, 2013, doi: 10.1109/ACCESS.2013.2260813.

[2] D. Caudill, J. Chuang, S. Y. Jun, C. Gentile, and N. Golmie, "Real-time mmWave channel sounding through switched beamforming with 3-D dual-polarized phased-array antennas," *IEEE Trans. Microw. Theory Techn.*, vol. 69, no. 11, pp. 5021–5032, Nov. 2021.

[3] T. S. Rappaport, J. N. Murdock, and F. Gutierrez, "State of the art in 60-GHz integrated circuits and systems for wireless communications," *Proc. IEEE*, vol. 99, no. 8, pp. 1390–1436, Aug. 2011, doi: 10.1109/JPROC.2011.2143650.

[4] S. Barrachina-Muñoz, B. Bellalta, and E. W. Knightly, "Wi-Fi channel bonding: An all-channel system and experimental study from urban hotspots to a sold-out stadium," *IEEE/ACM Trans. Netw.*, vol. 29, no. 5, pp. 2101–2114, Oct. 2021, doi: 10.1109/tnet.2021.3077770.

[5] J. D. Parsons, D. A. Demery, and A. M. D. Turkmani, "Sounding techniques for wideband mobile radio channels: A review," *IEE Proc. I Commun., Speech Vis.*, vol. 138, no. 5, pp. 437–446, Oct. 1991, doi: 10.1049/ip-i-2.1991.0059.

[6] D. Sugizaki, N. Iwakiri, and T. Kobayashi, "Ultra-wideband spatio-temporal channel sounding with use of an OFDM signal in an indoor environment," IEICE, Inst. Electron., Inf. Commun. Eng. (IEICE), Japan, Tech. Rep., pp. 47–52, 2010, vol. 110, no. 222.

[7] R. M. L. Silva, G. L. Siqueira, L. H. Gonsioroski, and C. R. V. Ron, "Comparison between OFDM and STDCC mobile channel sounders at 3.5 GHz," *J. Microw., Optoelectron. Electromagn. Appl.*, vol. 12, no. 1, pp. 1–14, Jun. 2013, doi: 10.1590/s2179-10742013000100001.

[8] T. Zwick, T. J. Beukema, and H. Nam, "Wideband channel sounder with measurements and model for the 60 GHz indoor radio channel," *IEEE Trans. Veh. Technol.*, vol. 54, no. 4, pp. 1266–1277, Jul. 2005, doi: 10.1109/tvt.2005.851354.

[9] C. Umit Bas, V. Kristem, R. Wang, and A. F. Molisch, "Real-time ultra-wideband frequency sweeping channel sounder for 3–18 GHz," in *Proc. IEEE Mil. Commun. Conf. (MILCOM)*, Oct. 2017, pp. 775–781, doi: 10.1109/MILCOM.2017.8170721.

[10] T. Srisooksai, J. I. Takada, and K. Saito, "Portable wide-band channel sounder based software defined radio for studying the radio propagation in an outdoor environment," in *Proc. Int. Symp. Antennas Propag. (ISAP)*, 2017, pp. 1–2, doi: 10.1109/ISANP.2017.8229040.

[11] J. Li, Y. Zhao, C. Tao, and B. Ai, "System design and calibration for wideband channel sounding with multiple frequency bands," *IEEE Access*, vol. 5, pp. 781–793, 2017, doi: 10.1109/access.2017.2649679.

[12] W. Rowe, P. Stoica, and J. Li, "Spectrally constrained waveform design [sp tips&tricks]," *IEEE Signal Process. Mag.*, vol. 31, no. 3, pp. 157–162, May 2014, doi: 10.1109/msp.2014.2301792.

[13] A. M. Khan, V. Jeoti, M. Z. U. Rehman, M. T. Jilani, O. Chugtai, and M. H. Rehmani, "Pilot-based time domain SNR estimation for broadcasting OFDM systems," *J. Comput. Netw. Commun.*, vol. 2018, pp. 1–8, May 2018, doi: 10.1155/2018/9319204.

[14] S. Coleri, M. Ergen, A. Puri, and A. Bahai, "Channel estimation techniques based on pilot arrangement in OFDM systems," *IEEE Trans. Broadcast.*, vol. 48, no. 3, pp. 223–229, Sep. 2002, doi: 10.1109/tbc.2002.804034.

[15] K. Medhat Nasr, J. P. Cosmas, M. Bard, and J. Gledhill, "Performance of an echo canceller and channel estimator for on-channel repeaters in DVB-T/H networks," *IEEE Trans. Broadcast.*, vol. 53, no. 3, pp. 609–618, Sep. 2007, doi: 10.1109/tbc.2007.903612.

[16] C. Chen and M. D. Zoltowski, "Bayesian sparse channel estimation," *Proc. SPIE*, vol. 8404, May 2012, Art. no. 84040A, doi: 10.1117/12.919302.

[17] S. Ariyavisitakul and J. Zheng, "Method and system for iterative discrete Fourier transform (DFT) based channel estimation using minimum mean square error (MMSE) techniques," U.S. Patent 8 750 089 B2, Jun. 10, 2014.

[18] W. Ding, F. Yang, C. Pan, L. Dai, and J. Song, "Compressive sensing based channel estimation for OFDM systems under long delay channels," *IEEE Trans. Broadcast.*, vol. 60, no. 2, pp. 313–321, Jun. 2014, doi: 10.1109/tbc.2014.2315913.

[19] C. Qi, G. Yue, L. Wu, and A. Nallanathan, "Pilot design for sparse channel estimation in OFDM-based cognitive radio systems," *IEEE Trans. Veh. Technol.*, vol. 63, no. 2, pp. 982–987, Feb. 2014, doi: 10.1109/tvt.2013.2280655.

[20] A. M. Khan, V. Jeoti, and M. A. Zakariya, "Improved pilot-based LS and MMSE channel estimation using DFT for DVB-T OFDM systems," in *Proc. IEEE Symp. Wireless Technol. Appl. (ISWTA)*, Sep. 2013, pp. 120–124, doi: 10.1109/ISWTA.2013.6688752.

[21] R. K. Mohammed, "Comparing various channel estimation techniques for OFDM systems using MATLAB," *Int. J. Wireless Mobile Netw.*, vol. 11, no. 3, Jun. 2019. [Online]. Available: https://ssrn.com/abstract=3420582 and http://dx.doi.org/10.2139/ssrn.3420582

[22] M. Zhu, "Low complexity channel estimation for OFDM based satellite systems," Ph.D. dissertation, Fac. Eng. Phys. Sci., Univ. Surrey, U.K., 2011.

[23] M. Bossert, A. Donder, and A. Trushkin, "Channel estimation and equalization in orthogonal frequency division multiplexing systems," *Mobile Kommunikation: ITG Fachtagung: Vorträge: Neu-Ulm*. Berlin, Germany:: VDE Verlag, 1995, pp. 26.09.95–28.09.95.

[24] M. J. Fernandez-Getino Garcia, J. M. Paez-Borrallo, and S. Zazo, "DFT-based channel estimation in 2D-pilot-symbol-aided OFDM wireless systems," in *Proc. IEEE VTS 53rd Veh. Technol. Conf.*, May 2001, pp. 810–814, doi: 10.1109/VETECS.2001.944491.

[25] Y. Zhao, W. Li, and W. Wu, "An efficient channel estimation method for OFDM systems with multiple transmit antennas," in *Proc. Int. Conf. Info-Tech Info-Net*, 2001, pp. 335–339, doi: 10.1109/ICII.2001.983600.

[26] A. A. Tahat and D. R. Ucci, "An extrapolated matched-filter approach to multi-user channel estimation for OFDM in SDMA," in *Proc. IEEE Antennas Propag. Soc. Int. Symp.*, Jun. 2002, pp. 636–639, doi: 10.1109/APS.2002.1016727.

[27] S. Sreenivasan, "DCT based channel estimation in OFDM using MMSE and LS," *Int. J. Eng. Res. Technol. (IJERT)*, vol. 8, no. 08, pp. 342–344, 2019.

[28] N. Sharma, V. Nandal, and D. Nandal, "Performance improvement using spline LS and MMSE DFT channel estimation technique in MIMO OFDM using block-type pilot structure," in *Data Analytics and Management*. Singapore: Springer, 2021, pp. 347–366.

[29] L. Tong, G. Xu, and T. Kailath, "Blind identification and equalization based on second-order statistics: A time domain approach," *IEEE Trans. Inf. Theory*, vol. 40, no. 2, pp. 340–349, Mar. 1994, doi: 10.1109/18.312157.

[30] S. Lu, A. Semmar, X. Wang, Y. Wu, J.-Y. Chouinard, and P. Fortier, "Implementation and field test of a new channel estimation technique for DVB-T system," in *Proc. Can. Conf. Electr. Comput. Eng.*, vol. 3, 2004, pp. 1343–1346, doi: 10.1109/CCECE.2004.1349648.

[31] M. Yu and P. Sadeghi, "Time domain synchronization and decoding of P1 symbol in DVB-T2," in *Proc. IEEE Int. Conf. Acoust., Speech Signal Process. (ICASSP)*, May 2011, pp. 3520–3523, doi: 10.1109/ICASSP.2011.5946237.

[32] A. M. Khan, V. Jeoti, M. Z. Ur Rehman, M. T. Jilani, and M. A. Zakariya, "A cyclic correlation-based time domain channel estimation scheme," in *Proc. 6th Int. Conf. Intell. Adv. Syst. (ICIAS)*, Aug. 2016, pp. 1–5, doi: 10.1109/ICIAS.2016.7824101.

[33] A. Iqbal, V. Jeoti, M. Drieberg, and W. Peng Wen, "A time-domain channel impulse response estimation method for an OFDM sounding system," in *Proc. IEEE Int. Conf. Smart Instrum., Meas. Appl. (ICSIMA)*, Aug. 2019, pp. 1–5, doi: 10.1109/ICSIMA47653.2019.9057303.

[34] H. Esmaiel and D. Jiang, "Spectrum and energy efficient OFDM multicarrier modulation for an underwater acoustic channel," *Wireless Pers. Commun.*, vol. 96, no. 1, pp. 1577–1593, Sep. 2017, doi: 10.1007/s11277-017-4257-5.

[35] N. Ur Rehman Junejo, H. Esmaiel, M. Zhou, H. Sun, J. Qi, and J. Wang, "Sparse channel estimation of underwater TDS-OFDM system using look-ahead backtracking orthogonal matching pursuit," *IEEE Access*, vol. 6, pp. 74389–74399, 2018, doi: 10.1109/ACCESS.2018.2881766.

[36] L. Dai, Z. Wang, and Z. Yang, "Compressive sensing based time domain synchronous OFDM transmission for vehicular communications," *IEEE J. Sel. Areas Commun.*, vol. 31, no. 9, pp. 460–469, Sep. 2013, doi: 10.1109/JSAC.2013.SUP.0513041.

[37] L. Dai, J. Wang, Z. Wang, P. Tsiaflakis, and M. Moonen, "Spectrum- and energy-efficient OFDM based on simultaneous multi-channel reconstruction," *IEEE Trans. Signal Process.*, vol. 61, no. 23, pp. 6047–6059, Dec. 2013, doi: 10.1109/TSP.2013.2282920.

[38] X. Wang, Y. Wu, J.-Y. Chouinard, S. Lu, and B. Caron, "A channel characterization technique using frequency domain pilot time domain correlation method for DVB-T systems," *IEEE Trans. Consum. Electron.*, vol. 49, no. 4, pp. 949–957, Nov. 2003, doi: 10.1109/tce.2003.1261180.

[39] M. Li, J. Tan, and W. Zhang, "A channel estimation method based on frequency-domain pilots and time-domain processing for OFDM systems," *IEEE Trans. Consum. Electron.*, vol. 50, no. 4, pp. 1049–1057, Nov. 2004, doi: 10.1109/TCE.2004.1362498.

[40] S. Liu, J. Zhan, W. Xie, and F. Li, "Channel estimation using frequency-domain superimposed pilot time-domain correlation method for OFDM systems," in *Proc. Int. Conf. Commun. Technol.*, Nov. 2006, pp. 1–4, doi: 10.1109/ICCT.2006.341841.

[41] K.-Y. Lin, H.-J. Huang, H.-P. Lin, and S.-S. Jeng, "Performance enhancement by applying FPTC and franks windowing in DVB-T receiver," in *Proc. IEEE Int. Symp. Broadband Multimedia Syst. Broadcast.*, Apr. 2008, pp. 1–4, doi: 10.1109/ISBMSB.2008.4536650.

[42] A. M. Khan, "Pilot-based time domain OFDM channel estimation for digital video broadcasting applications," Doctor Of Philosophy, Elect. Electron. Eng., Universiti Teknologi PETRONAS, Malaysia, 2016.

[43] H. A. Abbood, H. F. Khazal, and T. M. Jamel, "Time domain pilot-based channel estimation (TDPCE) using Kalman filtering for OFDM system," *IOP Conf. Ser., Mater. Sci. Eng.*, vol. 1090, no. 1, Mar. 2021, Art. no. 012064, doi: 10.1088/1757-899x/1090/1/012064.

[44] G. Cui, X. Yu, Y. Yang, and L. Kong, "Cognitive phase-only sequence design with desired correlation and stopband properties," *IEEE Trans. Aerosp. Electron. Syst.*, vol. 53, no. 6, pp. 2924–2935, Dec. 2017, doi: 10.1109/taes.2017.2721238.

[45] Z. Liu, Y. L. Guan, U. Parampalli, and S. Hu, "Spectrally-constrained sequences: Bounds and constructions," *IEEE Trans. Inf. Theory*, vol. 64, no. 4, pp. 2571–2582, Apr. 2018, doi: 10.1109/tit.2018.2800012.

[46] H. Steendam, "On the pilot carrier placement in multicarrier-based systems," *IEEE Trans. Signal Process.*, vol. 62, no. 7, pp. 1812–1821, Apr. 2014, doi: 10.1109/tsp.2014.2306179.

[47] K. Wesołowski, A. Langowski, and K. Bąkowski, "A novel pilot scheme for 5G downlink transmission," in *Proc. Int. Symp. Wireless Commun. Syst. (ISWCS)*, Aug. 2015, pp. 161–165, doi: 10.1109/ISWCS.2015.7454320.

[48] W. Pan, Z. Shan, T. Chen, F. Chen, and J. Feng, "Optimal pilot design for OFDM systems with non-contiguous subcarriers based on semi-definite programming," *Telecommun. Syst.*, vol. 63, no. 2, pp. 297–305, Oct. 2016, doi: 10.1007/s11235-015-0121-7.

[49] H. Singh and S. Bansal, *Pilot Subcarrier Based Channel Estimation in OFDM System* (Advanced Computational and Communication Paradigms). Singapore: Springer, 2018, pp. 84–91.

[50] F. Gao, T. Cui, and A. Nallanathan, "Scattered pilots and virtual carriers based frequency offset tracking for OFDM systems: Algorithms, identifiability, and performance analysis," *IEEE Trans. Commun.*, vol. 56, no. 4, pp. 619–629, Apr. 2008, doi: 10.1109/tcomm.2008.060050.

[51] Q. Huang, M. Ghogho, and S. Freear, "Pilot design for MIMO OFDM systems with virtual carriers," *IEEE Trans. Signal Process.*, vol. 57, no. 5, pp. 2024–2029, May 2009, doi: 10.1109/tsp.2008.2011824.

[52] S. Sreepada and S. Kalyani, "Channel estimation in OFDM systems with virtual subcarriers using DPSS," *IEEE Commun. Lett.*, vol. 20, no. 12, pp. 2462–2465, Dec. 2016, doi: 10.1109/lcomm.2016.2608353.

[53] J. Haifang and S. Yin, "An efficient iterative DFT-based channel estimation for MIMO-OFDM systems on multipath channels," in *Proc. 3rd Int. Conf. Commun. Netw. China*, Aug. 2008, pp. 45–49, doi: 10.1109/CHINACOM.2008.4684966.

[54] H. Ali and A. Rahim Leyman, "An iterative DFT-based channel estimation algorithm for OFDM systems with virtual carriers," in *Proc. 26th IEEE Can. Conf. Electr. Comput. Eng. (CCECE)*, May 2013, pp. 1–5, doi: 10.1109/CCECE.2013.6567744.

[55] A. Iqbal, V. Jeoti, M. Drieberg, and W. Peng Wen, "Chu sequence based phasing scheme for low PAPR multicarrier waveform for channel sounding," in *Proc. IEEE 30th Can. Conf. Electr. Comput. Eng. (CCECE)*, May 2017, pp. 1–4, doi: 10.1109/CCECE.2017.7946762.

[56] W. P. Siriwongpairat and K. R. Liu, *Ultra-Wideband Communications Systems: Multiband OFDM Approach*. Hoboken, NJ, USA: Wiley, 2007.

[57] M. Morelli and U. Mengali, "A comparison of pilot-aided channel estimation methods for OFDM systems," *IEEE Trans. Signal Process.*, vol. 49, no. 12, pp. 3065–3073, Dec. 2001, doi: 10.1109/78.969514.

**ASIF IQBAL** received the M.Sc. and Ph.D. degrees in electrical and electronic engineering from Universiti Teknologi PETRONAS (UTP), Malaysia. He has over 15 years of experience in research and development, specializing in the IoT, sensor systems, and wireless communication technologies. His notable achievements include leading a patented maritime communication technology and pioneering research in tropospheric radio wave propagation modeling at UTP. His research interests include fast and efficient numerical algorithms, radio propagation, wireless channel characterization, and modeling. He is currently working on the channel sounder and emulators.

**MICHEAL DRIEBERG** (Member, IEEE) received the B.Eng. degree in electrical and electronics engineering from Universiti Sains Malaysia, Penang, Malaysia, in 2001, the M.Sc. degree in electrical and electronics engineering from Universiti Teknologi PETRONAS (UTP), Seri Iskandar, Malaysia, in 2005, and the Ph.D. degree in electrical and electronics engineering from Victoria University, Melbourne, Australia, in 2011. He is currently a Senior Lecturer with the Department of Electrical and Electronics Engineering, UTP. He has made several contributions to the Wireless Broadband Standards Group. He has published and served as a reviewer for several high impact journals and flagship conferences. His research interests include radio resource management, medium access control protocols, energy harvesting communications, and performance analysis for wireless and sensor networks.

**VARUN JEOTI** (Senior Member, IEEE) received the Ph.D. degree from the Indian Institute of Technology Delhi, Delhi, India, in 1992. He has over 29 years of teaching experience in leading Indian and Malaysian universities teaching students from various social and cultural backgrounds. He has been conducting frontier research for over 38 years in the area of surface acoustic wave (SAW) devices, signal processing, and wireless communication. In 1980, after his graduation from IIT Delhi, he worked on government sponsored projects developing SAW Pulse compression filters, and underwater optical receivers with IIT Madras. He was a Visiting Faculty with the Electronics Department, Madras Institute of Technology, Anna University, from 1989 to 1990, and then he joined the Delhi Institute of Technology, until 1995. He moved to the School of Electrical and Electronic Engineering (E. & E. Engg.), Universiti Sains Malaysia, in 1995, and later moved to the Department of Electrical and Electronic Engineering, Universiti Teknologi PETRONAS, in 2001. He is currently with the Faculty of Technical Sciences, University of Novi Sad, Serbia, as an ERA Chair leading research efforts in stretchable and textile electronics. His research interests include, among others, signal processing, SAW sensor-tags, SAW microfluidics, and wireless communication for various applications.

**AZRINA ABD AZIZ** (Senior Member, IEEE) received the bachelor's degree (Hons.) in electrical and electronic engineering from The University of Queensland, Australia, in 1997, the M.Sc. degree in system level integration from the Institute for System Level Integration (ISLI), Scotland, in 2003, and the Ph.D. degree in computer systems engineering from Monash University, Melbourne, Australia, in 2013. She is currently a Senior Lecturer with the Department of Electrical and Electronic Engineering, Universiti Teknologi PETRONAS (UTP), Malaysia. Prior to her academic appointment, she worked briefly in industry handling the final visual inspection process of IC packaging. Her current research interests include energy-efficient techniques for topology control in wireless sensor networks (WSNs), wireless body area networks (WBANs) for biomedical applications and medical imaging, and machine learning techniques. She is also leading the SMART Assistive and Rehabilitation Technology Research Group, UTP. She is a member of Board of Engineers Malaysia. She is holding the positions of the Treasurer of IEEE Robotics and Automation Society and the Chair-Elect of IEEE Women in Engineering Malaysia. She is a Reviewer of *Ad Hoc Networks* journal (ScienceDirect).

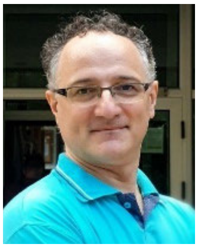

**GORAN M. STOJANOVIĆ** (Member, IEEE) received the B.Sc., M.Sc., and Ph.D. degrees in electrical engineering from the Faculty of Technical Sciences (FTS), University of Novi Sad (UNS), Serbia, in 1996, 2003, and 2005, respectively. He is currently a Full Professor with FTS-UNS. He has 26 years of experience in research and development. His research interests include sensors, flexible electronics, textile electronics, and microfluidics. He is the author/coauthor of 260 articles, including 107 in leading peer-reviewed journals with impact factors, five books, three patents, one chapter in monograph. He is a keynote speaker for 12 international conferences. He has been a supervisor of 11 Ph.D. students, 40 M.Sc. students, and 60 diploma students with FTS-UNS. He has more than 14 year's experience in coordination of EU funded projects (H2020, FP7, EUREKA, ERASMUS, and CEI), with total budget exceeding 14.86 MEUR. He also coordinates four Horizon2020 projects in the field of green electronics and textile electronics.

**MITAR SIMIĆ** (Member, IEEE) was born in Ljubovija, Serbia, in 1987. He received the B.Sc. and M.Sc. degrees in electrical engineering from the University of East Sarajevo, Bosnia and Herzegovina, in 2010 and 2012, respectively, and the Ph.D. degree in electrical engineering from the University of Novi Sad, Serbia in 2017. He is a Postdoctoral Researcher within the STRENTEX project at the Faculty of Technical Sciences, University of Novi Sad. He is an author/coauthor of 38 scientific papers in leading peer-reviewed journals with impact factor. His research interests include sensors, impedance spectroscopy analysis, equivalent circuit modeling, and development of devices for impedance measurement and data acquisition.

**NAZABAT HUSSAIN** received the M.Sc. and Ph.D. degrees in electrical and electronics engineering from Universiti Teknologi PETRONAS, Malaysia. Currently, he is a Research and Development Engineer with GE Vingmed Ultrasound AS. He is specialized in computational algorithms, image processing, signal processing, AI, embedded system, wireless communication, and applied electromagnetics. He has published his research work indexed journals/conferences.